Journal of Power Sources 185 (2008) 1374–1379

Contents lists available at ScienceDirect

Journal of Power Sources

journal homepage: www.elsevier.com/locate/jpowsour

Effects of vanadium- and iron-doping on crystal morphology and electrochemical properties of 1D nanostructured manganese oxides

Ha Na Yoo, Dae Hoon Park, Seong-Ju Hwang*

Center for Intelligent Nano-Bio Materials (CINBM), Department of Chemistry and Nano Sciences, Ewha Womans University, Seoul 120-750, Republic of Korea

ARTICLE INFO

Article history:
Received 23 May 2008
Received in revised form 14 July 2008
Accepted 21 August 2008
Available online 6 September 2008

Keywords:
1D nanostructure
Manganese oxide
Cation doping
Aspect ratio
Electrode performance
Lithium-ion battery

ABSTRACT

One-dimensional (1D) nanostructures of vanadium- and iron-doped manganese oxides, $Mn_{1-x}M_xO_2$ (M = V and Fe), are synthesized via one-pot hydrothermal reactions. The results of X-ray diffraction studies and electron microscopic analyses demonstrate that all the present 1D nanostructured materials possess α-MnO_2-type structure. While the vanadium dopants produce 1D nanorods with a smaller aspect ratio of ~3–5, iron dopants produce 1D nanowires with a high aspect ratio of >20. X-ray absorption spectroscopy clearly shows that the dopant vanadium ions are stabilized in tetravalent oxidation state with distorted octahedral symmetry, while the iron ions are stabilized in trivalent oxidation state with regular octahedral symmetry. Significant local structural distortion and size mismatch of dopant vanadium ions are responsible for the low aspect ratio of the vanadium-doped nanorods through the less effective growth of a 1D nanostructure. According to electrochemical measurements, doping with Fe and V can improve the electrode performance of 1D nanostructured manganate and such a positive effect is much more prominent for the iron dopant. The present study clearly indicates that doping with Fe and V provides an effective way of tailoring the crystal dimension and electrochemical properties of 1D nanostructured manganese oxides.

1. Introduction

Over the past decades, manganese oxides have received considerable attention because of their promising functionality as electrodes for lithium-ion batteries and supercapacitors, redox catalysts, bio-sensors, and so on [1–5]. Research on manganese oxides has been extended to one-dimensional (1D) nanostructured homologues and three-dimensional (3D) assemblies [6–11]. It is well known that the functionality of bulk manganese oxide can be optimized by the partial substitution of Mn with other metal ions [1]. In light of this, several attempts have been made to substitute a fraction of manganese ions in the nanostructured manganate with other transition metal ions [12–14]. However, in general, the chemical substitution is quite difficult for nanostructured manganese oxides compared with their bulk counterparts whose compositions can be easily tailored by changing the mixing ratio of solid-state reactants. Recently, we were successful [14–18] in preparing Cr-, Al-, Ni-, and Co-substituted manganese oxide nanowires through the redox reactions of solid-state precursors or ion-adduct precursors under hydrothermal or non-hydrothermal condition. It was found that the partial replacement of Mn with transition metal ions could improve the electrode performance of 1D nanostructured manganates [15–17]. According to X-ray absorption spectroscopic (XAS) studies, manganese ions in these nanostructured compounds are commonly stabilized in octahedral sites with a trivalent or tetravalent oxidation state. Considering the preference of transition metal ions for a specific oxidation state, iron and vanadium ions are expected to be as suitable dopants for 1D nanostructured manganate. Moreover, iron ions have a strong preference for octahedral symmetry, whereas vanadium ions can be stabilized in various local symmetries from octahedra to square planar geometry [19]. In this regard, it would be very interesting to investigate the effects of the local symmetry of dopant metal ions on the crystal morphology and electrochemical properties of 1D nanostructured manganese oxides. To date, however, there have been no reports concerning the doping of 1D nanostructured manganates with vanadium and iron ions.

In this study, we have synthesized successfully V- and Fe-doped manganese oxide nanowires via a one-pot hydrothermal reaction of a mixed solution of metal components and oxalate ligands. The effects of vanadium- and iron-doping on the chemical bonding nature and crystal morphology of the 1D nanostructured manganates have been investigated by means of a combination of microscopic and spectroscopic tools. The nanostructured materials are evaluated as intercalation electrodes for lithium secondary batteries to examine the influence of cation doping on the electrochemical properties of manganese oxide nanostructures.

* Corresponding author. Tel.: +82 2 3277 4370; fax: +82 2 3277 3419.
E-mail address: hwangsju@ewha.ac.kr (S.-J. Hwang).

0378-7753/$ – see front matter © 2008 Elsevier B.V. All rights reserved.
doi:10.1016/j.jpowsour.2008.08.085

2. Experimental

2.1. Synthesis

The 1D nanostructures of the vanadium- and iron-doped manganese oxides, $Mn_{1-x}M_xO_2{\cdot}yH_2O$ (M = V and Fe), were prepared by the hydrothermal treatment of a mixture solution of manganese(II) sulfate (4×10^{-3} mol), iron(III) nitrate hemipentahydrate or vanadium(III) chloride (4×10^{-4} mol), oxalic acids (2×10^{-2} mol), and ammonium persulfate (2.5×10^{-2} mol) at 180 °C for 40 h. The pH of the reactant solution was adjusted to pH 5. To promote the incorporation of dopant ions into the lattice of manganese oxide, oxalate chelate ligands were added to the mixed solution of metal ions. For the both dopants, the mole ratio of M:Mn was fixed at 1:10. The obtained powdery samples were washed thoroughly with distilled water and dried in an oven at 50 °C.

2.2. Characterization

The crystal structures of the present nanostructured manganates were characterized by powder X-ray diffractometer (XRD, Rigaku, λ = 1.54059 Å, 298 K) measurements. Their thermal behaviour was studied by performing thermogravimetric analysis (TGA) under ambient atmosphere at the rate of 10 °C min^{-1}. The crystal morphology and cation composition of the nanostructured materials were examined by field emission-scanning electron microscopy (FE-SEM, JEOL JSM-6700F) with an energy-dispersive X-ray spectrometer (EDS). The crystal dimensions of the manganates were examined using high resolution-transmission electron microscopy (HR-TEM, Philips-CM200, 200 kV) microscope. The XAS experiments were carried out with the extended X-ray absorption fine structure (EXAFS) facility installed on beam line 7C at the Pohang Accelerator Laboratory (PAL) in Korea. The data were collected at room temperature in a transmission mode using gas-ionization detectors. All the spectra were calibrated by simultaneously measuring the spectrum of manganese, vanadium, or iron metal foil. Analysis of the experimental spectra was performed by the standard procedure reported previously [20].

2.3. Electrode performance test

Electrochemical measurements were performed with a cell of Li/1M $LiPF_6$ in ethylene carbonate (EC):diethyl carbonate (DEC) (50:50, v/v)/composite cathode, that was assembled in an Ar-filled glove box. 20 mg of active electrode material was mixed with 12 mg of conductive binder (i.e., 8 mg of teflonized acetylene black and 4 mg of graphite). All experiments were carried out in a galvanostatic mode with a Maccor multichannel galvanostat/potentiostat. The measurements were performed in the voltage range of 1.0–4.3 V at a constant current density 20 mA g^{-1}.

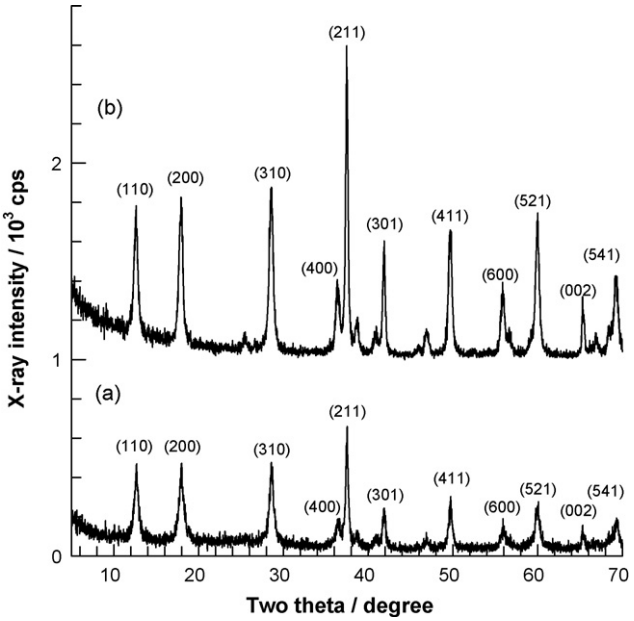

Fig. 1. Powder XRD patterns of 1D nanostructured α-$Mn_{1-x}M_xO_2$ with M = (a) V and (b) Fe.

3. Results and discussion

3.1. Powder XRD, EDS, and TGA measurements

The powder XRD patterns of vanadium- and iron-doped manganese oxides are presented in Fig. 1. Both the cation-doped manganates showed a series of sharp Bragg reflections, which can be well indexed to α-MnO_2 structure containing 2 × 2 pores [15]. Between the two compounds, the Fe-doped manganate displays diffraction peaks with higher intensities than the V-doped sample. This reflects the better crystallinity of the former phase. According

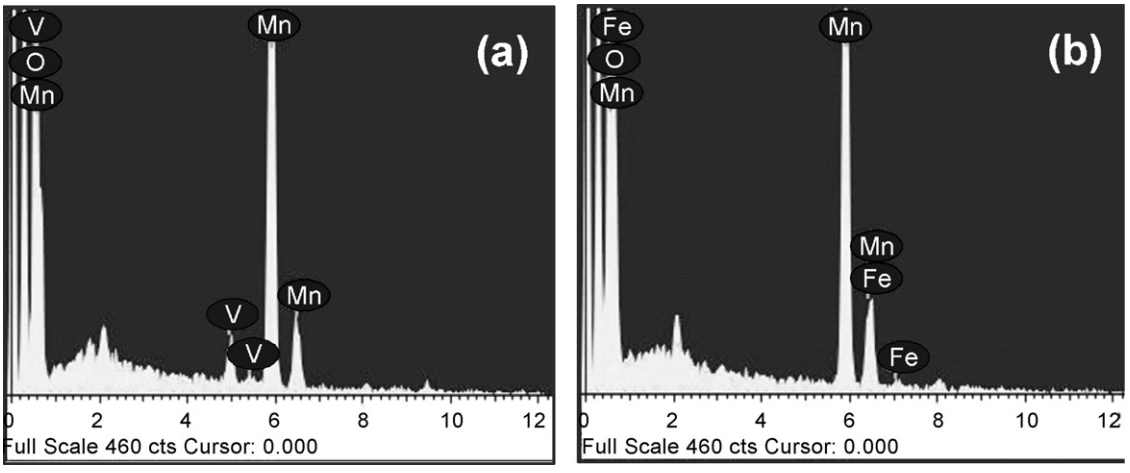

Fig. 2. EDS data of 1D nanostructured α-$Mn_{1-x}M_xO_2$ with M = (a) V and (b) Fe.

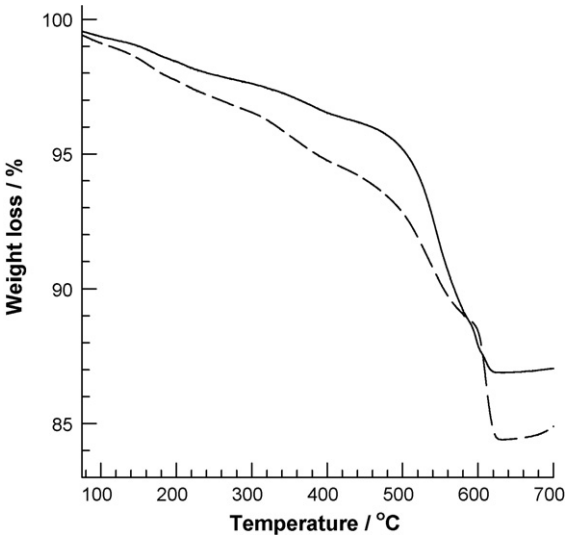

Fig. 3. TGA curves of 1D nanostructured α-$Mn_{1-x}M_xO_2$ with M = V (dashed lines) and Fe (solid lines).

to least squares fitting analysis, the unit cell volume of the manganese oxide is slightly expanded by the partial replacement of Mn with V or Fe (a = 9.856 Å, c = 2.856 Å for α-$Mn_{1-x}V_xO_2$; a = 9.875 Å, c = 2.868 Å for α-$Mn_{1-x}Fe_xO_2$; a = 9.785 Å, c = 2.863 Å for α-MnO_2), which can be attributed to the larger size of dopant V^{4+} and Fe^{3+} ions with respect to Mn^{4+} ions [21]. This is considered as strong evidence of V- and Fe-doping in the manganate lattice. The incorporation of V and Fe ions into manganese oxides is cross-confirmed by EDS data. As illustrated in Fig. 2, EDS peaks corresponding to vanadium or iron ions are clearly observed together with Mn-related peaks. From the EDS analysis, the substitution rate of M/Mn is determined to be 0.05 for M = V and 0.14 for M = Fe, respectively, even though the M:Mn ratio is fixed to 0.1. This finding indicates the higher doping efficiency of the iron ion.

The water contents of the present manganese oxide nanostructures were estimated using TGA technique. As shown in Fig. 3, the V- and Fe-doped manganates exhibit considerable weight losses of 2.0 and 1.5% in the temperature range of 100–250 °C, respectively, which correspond to a water content of 0.26 and 0.20 per unit formula.

3.2. FE-SEM and TEM analyses

The FE-SEM images of the vanadium- and iron-doped manganese oxides are shown in Fig. 4. The vanadium-doped manganese oxide has 1D nanorod-type morphology with a diameter of ~15–30 nm and a length of ~100 nm. On the other hand, a much higher aspect ratio is obtained for the iron-doped manganate with the diameter of ~30–70 nm and the length of several micrometers. Such a variation in crystal morphology suggests that the crystal growth along the c-axis is more retarded by V-doping than by Fe-doping. This can be attributed to the greater mismatch of ionic size between V^{4+} and Mn^{4+} ions, compared with that between Fe^{3+} and Mn^{4+} ions [21]. The structural difference from vanadium-doping is cross-confirmed by the low substitution efficiency of vanadium ions for the manganate lattice, in which the amount of vanadium incorporated (x = 0.05) is approximately one-third of that of iron ions (x = 0.14). Further evidence of formation of the 1D nanostructures is obtained by TEM analysis, as illustrated in Fig. 5. The observed dimensions of the nanostructured materials are compatible with the FE-SEM data presented here (Fig. 4).

3.3. Mn K-, V K- and Fe K-edge XANES analyses

The Mn K-edge X-ray absorption near-edge structure (XANES) spectra of the V- and Fe-doped manganese oxide 1D nanostructures are illustrated in Fig. 6, together with those of $LiMn_{0.9}Cr_{0.1}O_2$ and λ-MnO_2. The edge energies of the nanostructured manganates are slightly lower than that of the reference λ-$Mn^{4+}O_2$, but higher than that of $LiMn_{0.9}{}^{3+}Cr_{0.1}O_2$. This is indicative of the mixed oxidation states of Mn^{3+}/Mn^{4+} in these compounds. In the pre-edge region, both the nanostructured manganese oxides display weak features P and P′ that are assigned as dipole-forbidden 1s → 3d transitions [20,22]. Since these transitions are not allowed by the dipole selection rule, the weak intensity of the pre-edge features provides strong evidence of the stabilization of manganese ions in the octahedral site with an inversion centre [22]. In the main-edge region, there are several peaks A, B, and C that correspond to dipole-allowed 1s → 4p transitions. In comparison with the reference bulk manganese oxides, spectral feature A in the middle of edge jump is much weaker for the V- and Fe-doped manganates, which is a characteristic of a nanocrystalline metal oxide [22]. In addition, the V- and Fe-doped manganates commonly demonstrate a rather broad and diffuse peak C. Given the fact that the sharpness and intensity of this peak are proportional to the relative concentration

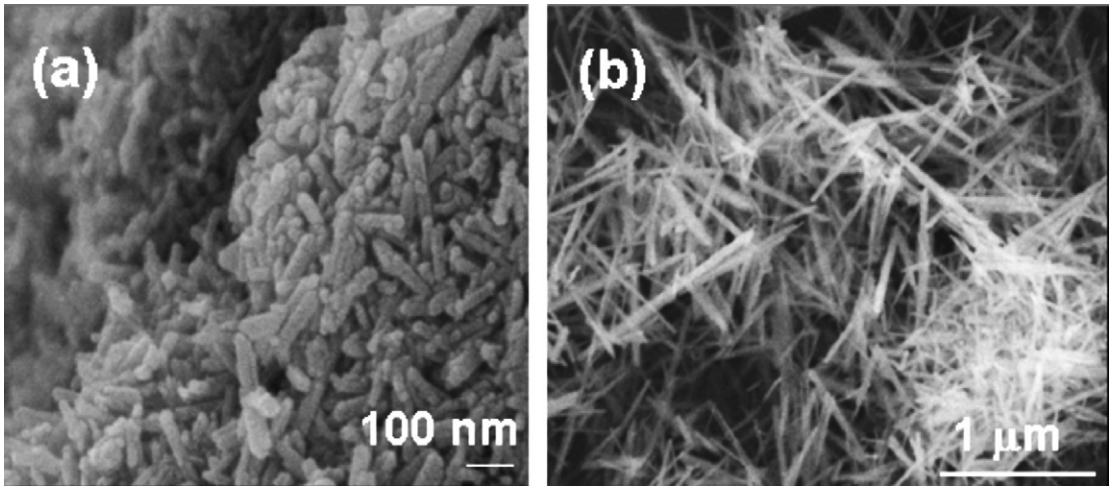

Fig. 4. FE-SEM images of 1D nanostructured α-$Mn_{1-x}M_xO_2$ with M = (a) V and (b) Fe.

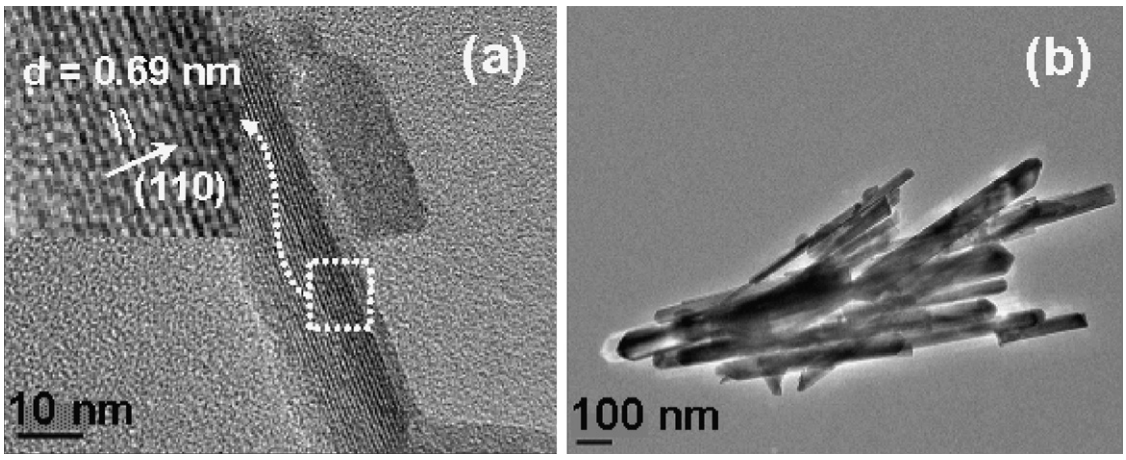

Fig. 5. HR-TEM images of 1D nanostructured α-$Mn_{1-x}M_xO_2$ with M = (a) V and (b) Fe.

of edge-sharing over corner-sharing of MnO_6 octahedra [23], the observed broad feature of the peak C is in good agreement with the α-MnO_2-type structure of the present manganates. This structure is composed of corner- and edge-sharing of MnO_6 octahedra. In this context, a sharp and intense peak C in the spectra of $LiMn_{0.9}Cr_{0.1}O_2$ and λ-MnO_2 can be verified with their crystal structures composed of edge-shared MnO_6 octahedra only.

The V K-edge XANES spectra of the vanadium-doped manganese oxide are shown in Fig. 7, together with those of the references V_2O_3, V_2O_4, and V_2O_5. The edge energy of the vanadium-doped manganese oxide is higher than that of the reference $V_2^{3+}O_3$, but similar to that of the reference $V_2^{4+}O_4$. Moreover, the references V_2O_4 and V_2O_5 show notable differences in terms of the positions and shapes of the main-edge features A, B, and C corresponding to the 1s → 4p transitions. As can be seen from Fig. 7, the overall spectral feature of the V-doped manganate is closer to that of the reference V_2O_4, compared with that of the reference V_2O_5. This is considered as significant evidence for the tetravalent oxidation of dopant vanadium ions. Similar to the Mn K-edge, all the present compounds display a pre-edge peak P related to the 1s → 3d transition. Although this transition is not allowed by the dipole selection rule, these peaks can be enhanced by the distortion of V local symmetry from centrosymmetric octahedra to non-centrosymmetric tetrahedra due to the mixing between p and d orbitals [22]. Thus the intensity of this peak could provide a sensitive probe for the local structure of absorbing vanadium ions. Only a weak pre-edge peak P appear for the reference V_2O_3 with a corundum structure, which is well consistent with the fact that the vanadium ions in this structure exist in octahedral geometry [19]. By contrast, the reference V_2O_4 and V_2O_5 compounds exhibit a higher intensity for this pre-edge peak P, which is in good agreement with their severely distorted octahedral geometry and penta-coordination geometry of vanadium ions [19,24]. In comparison with the references V_2O_4 and V_2O_5, the vanadium-doped manganate exhibits a lower intensity for this peak P, suggesting an octahedral-like geometry of vanadium ions; the height of this peak is determined to be 0.44 for α-$Mn_{1-x}V_xO_2$, 0.56 for V_2O_4, and 0.52 for V_2O_5. It is noteworthy that the intensity of the pre-edge peak P is quite higher for the V K-edge data of the vanadium-doped manganate compared with the corresponding Mn K-edge data. This provides strong evidence for the presence of significant structural distortion around vanadium ions in this compound. This conclusion is further supported by the

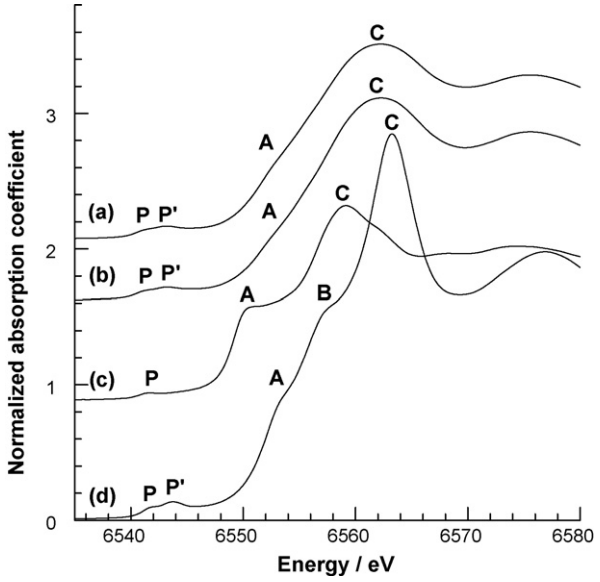

Fig. 6. Mn K-edge XANES spectra for 1D nanostructured α-$Mn_{1-x}M_xO_2$ with M = (a) V and (b) Fe, (c) $LiMn_{0.9}Cr_{0.1}O_2$, and (d) λ-MnO_2.

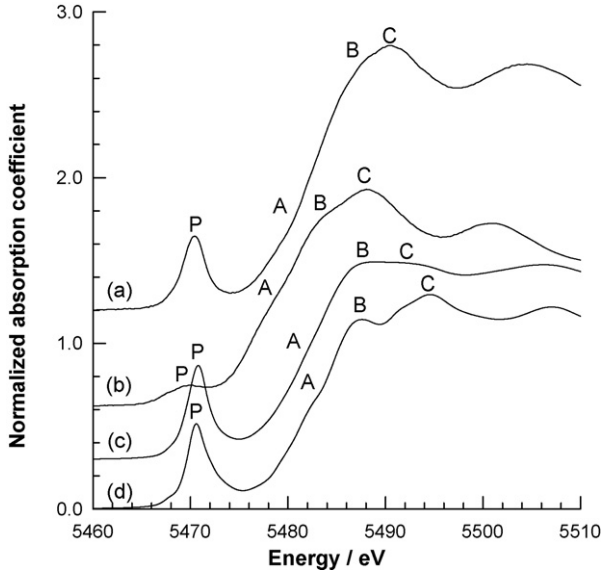

Fig. 7. V K-edge XANES spectra for (a) 1D nanostructured α-$Mn_{1-x}V_xO_2$, (b) V_2O_3, (c) V_2O_4, and (d) V_2O_5.

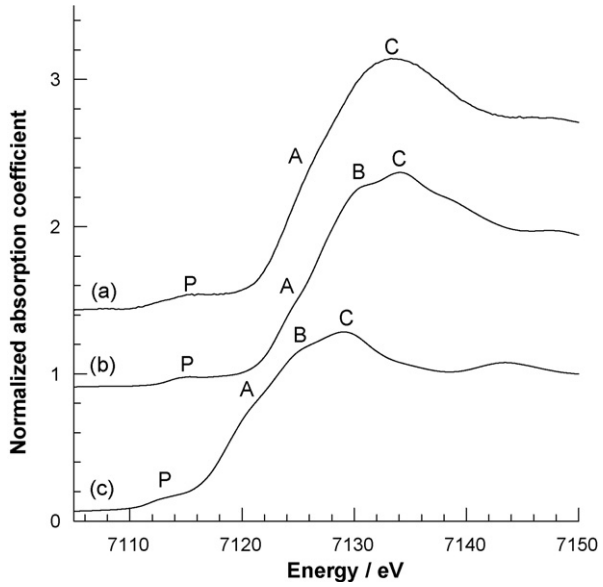

Fig. 8. Fe K-edge XANES spectra for (a) 1D nanostructured α-$Mn_{1-x}Fe_xO_2$, (b) Fe_2O_3, and (c) Fe_3O_4.

fact that the common symmetry of tetravalent vanadium ions in the oxide structure is either distorted octahedral or square pyramidal geometry [19,25].

Fig. 8 plots the Fe K-edge XANES spectra of the iron-doped manganese oxide, Fe_3O_4, and Fe_2O_3. The edge energy of the Fe-doped manganese oxide was approximately similar to that of the reference $Fe_2{}^{3+}O_3$, suggestive of the presence of trivalent iron ions. The incorporation of iron ions into the octahedral manganese site is obviously verified by the weak intensity of the pre-edge peak P corresponding to the dipole-forbidden $1s \rightarrow 3d$ transition [22]. It is noteworthy here that the local atomic arrangement of the iron dopant shows a higher degree of structural order than that of the vanadium ion. The greater structural disorder of vanadium ions allows us to explain not only the observed low doping efficiency of the V-doped manganate but also the low aspect ratio of V-doped manganate nanostructures. That is, notably different local symmetry of vanadium and manganese ions creates significant strain in the crystal structure of manganate lattice upon the V-doping, leading to the prevention of effective crystal growth of the V-doped manganate nanowires.

3.4. Electrochemical measurements

The effects of vanadium- and iron-doping on the electrode performance of 1D nanostructured manganese oxides have been examined via electrochemical measurements of the V- and Fe-doped α-MnO_2 nanostructures. For comparison, we also have prepared undoped α-MnO_2 nanowires and measured their electrochemical properties as lithium intercalation electrodes. As shown in Fig. 9, all the nanostructured manganates under investigation display smoother potential curves, which is a characteristic of nanocrystalline electrode materials [22]. The discharge capacities of the undoped, vanadium- and iron-doped manganese oxides are plotted in Fig. 10 as a function of cycle number. In comparison with the undoped α-MnO_2 nanowire, the V- and Fe-doped materials give better electrode performance for all the present cycles. Between both cation-doped manganates, the Fe-doped sample exhibits much larger discharge capacity with weaker capacity fading; the Fe-doped compound has larger discharge capacities of ~242 and ~205 mAh g^{-1} for the 10th and 50th cycle, respec-

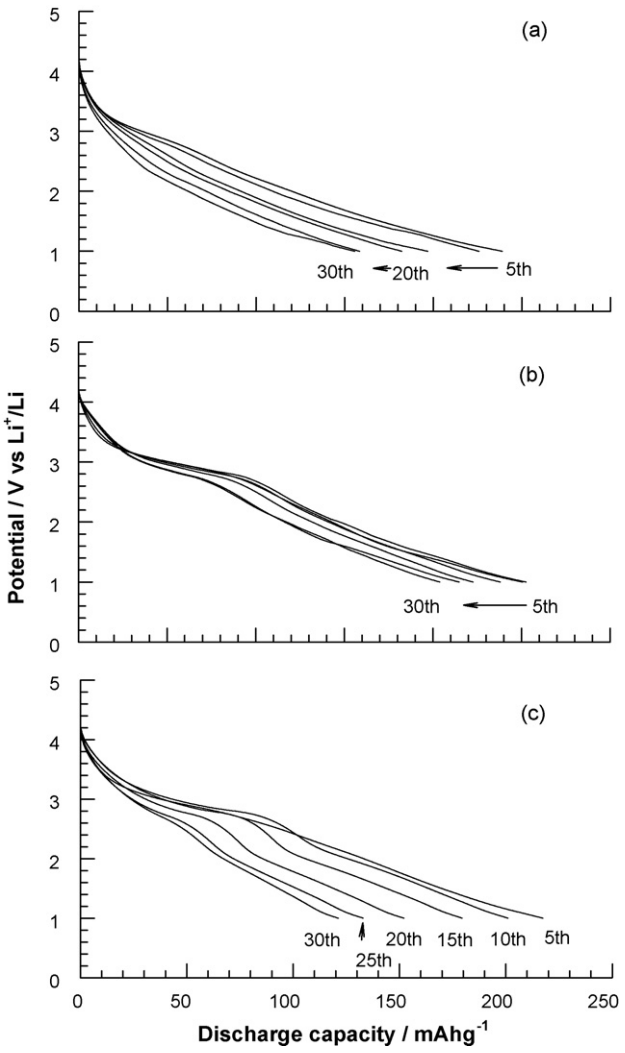

Fig. 9. Potential profiles of 1D nanostructured α-$Mn_{1-x}M_xO_2$ with M = (a) V and (b) Fe, and (c) α-MnO_2 nanowires for 5th, 10th, 15th, 20th, 25th, and 30th cycle.

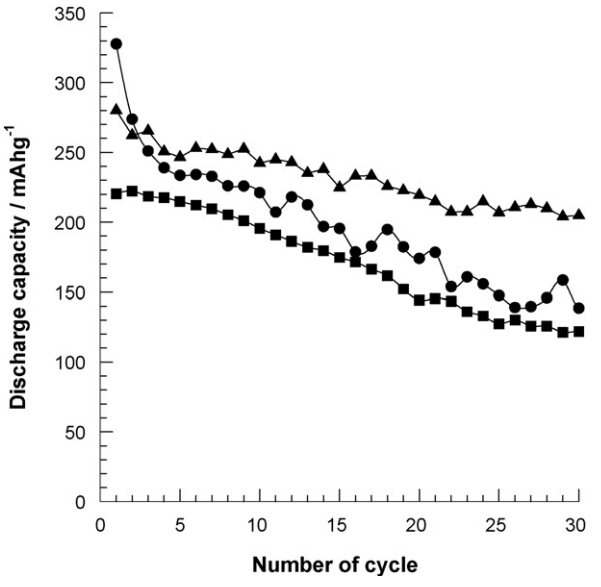

Fig. 10. Discharge capacity plots of 1D nanostructured α-$Mn_{1-x}M_xO_2$ with M = V (circles), and Fe (triangles), and α-MnO_2 nanowires (squares).

tively, compared with the V-doped (~221 and ~139 mAh g^{-1}) and the undoped manganates (~195 and ~122 mAh g^{-1}). This finding clearly demonstrates that doping with iron or vanadium ions is very useful for improving the electrochemical properties of 1D nanostructured manganese oxides. It is interesting that, in contrast to the present results regarding the nanostructured manganese oxide, V-doping does not increase the discharge capacity of bulk lithium manganese oxide [26]. The different influence of V-doping on the electrochemical performance of nanocrystalline and microcrystalline manganese oxides is related to the higher stability of the nanocrystals to accommodate various types of dopants [22]. By contrast the Fe-doping is commonly effective in improving the electrode performances of both bulk and nanostructured manganates [27]. This is attributed to the improvement of crystallinity and the negligible structural distortion caused by Fe-doping. The present finding strongly suggests that the iron-doped manganate has a high structural tolerance with respect to the electrochemical Li^+ insertion–extraction process. By contrast, the dopant vanadium ion is found to have a distorted local symmetry from regular octahedron [19], which causes significant structural strain in the crystal lattice of the α-MnO_2 phase. Moreover, it is well known that the vanadium ion experiences remarkable local structural variations from tetrahedral to octahedral symmetry during decrease of the oxidation state of vanadium [25]. Consequently, the vanadium-doped manganate will suffer from severe structural modifications during electrochemical cycling, which is responsible for its poorer electrode performance compared with the iron-doped sample. In addition, in contrast to the tetravalent oxidation state of the vanadium ions, the dopant iron ions have a trivalent oxidation state, as determined from the XANES results. The replacement of Fe^{3+} ions for Mn^{3+}/Mn^{4+} ions gives rise to an increase in the average Mn oxidation state and hence to the removal of unstable Mn^{3+} ions [28]. In this regard, such evolution of the electronic structure on the Fe-doping also improves the electrochemical performance of the Fe-doped manganate nanostructure. From the present experimental findings, it is obvious that the partial replacement of manganese ions with iron or vanadium is beneficial in terms of improving the electrode performance of 1D manganese oxide nanostructures.

4. Conclusions

The 1D nanostructures of vanadium- and iron-doped α-$Mn_{1-x}M_xO_2$ (M = V and Fe) have been synthesized by one-pot hydrothermal reactions. The results of FE-SEM and TEM analyses show that the aspect ratio of the 1D nanostructured manganese oxides is effectively controlled through the doping of vanadium and iron ions. This can be attributed to a limitation in the crystal growth of manganese oxide by the incorporation of vanadium ions with different local symmetries and dissimilar ionic sizes. XANES analyses at Mn K-, V K-, and Fe K-edges reveal that the tetravalent V^{4+} and trivalent Fe^{3+} ions are substituted into the manganese sites of the α-MnO_2 structure and the former ions induce significant local structural distortion from regular octahedral symmetry. Doping with Fe and V is found to improve the electrode performance of 1D nanostructured manganate and the positive effect of cation doping is more distinct for the iron ions. Such an improvement in the electrode performance of manganese oxides upon the Fe doping can be understood by an improvement in the structural stability and crystallinity as well as by a lowering of the concentration of unstable Mn^{3+} ions. In conclusion, doping with Fe and V enables control of the crystal morphology and electrochemical performance of 1D nanostructured manganese oxides.

Acknowledgments

This work was supported by a grant (20070401034003) from the BioGreen 21 Program and partly by a Korean Science and Engineering Foundation (KOSEF) grant funded by the Korea government (MEST) (grant: R11-2005-008-00000-0). The experiments at Pohang Accelerator Laboratory (PAL) were supported in part by MOST and POSTECH.

References

[1] M.M. Thackeray, Prog. Solid State Chem. 25 (1997) 1.
[2] F. Cheong, J. Zhao, W. Song, C. Li, H. Ma, J. Chen, P. Shen, Inorg. Chem. 45 (2006) 2038.
[3] M. Toupin, T. Brousse, D. Belanger, Chem. Mater. 16 (2004) 3184.
[4] P.B. Weisz, J. Catal. 10 (1968) 407.
[5] A.L. Cabrera, M.B. Maple, G. Arrhenius, Appl. Catal. 64 (1990) 309.
[6] X. Wang, X. Wang, W. Huang, P.J. Sebastian, S. Gamboa, J. Power Sources 140 (2005) 211.
[7] C.S. Johnson, J. Power Sources 165 (2007) 559.
[8] N. Wang, L. Guo, L. He, X. Cao, R. Wang, S. Yang, Small 3 (2007) 606.
[9] G.-Y. Zhao, C.-L. Xu, H.L. Li, J. Power Sources 163 (2007) 1132.
[10] T.D. Xiao, P.R. Strutt, M. Benaissa, H. Chen, B.H. Kear, Nanostruct. Mater. 10 (1998) 1051.
[11] X. Wang, Y. Li, J. Am. Chem. Soc. 124 (2002) 2880.
[12] J. Liu, Y.-C. Son, J. Cai, X. Shen, S.L. Suib, M. Aindow, Chem. Mater. 16 (2004) 276.
[13] J. Cai, J. Liu, W.S. Willis, S.L. Suib, Chem. Mater. 13 (2001) 2413.
[14] D.H. Park, S.T. Lim, S.-J. Hwang, C.-S. Yoon, Y.K. Sun, J.-H. Choy, Adv. Mater. 17 (2005) 2834.
[15] D.H. Park, S.-H. Lee, T.W. Kim, S.T. Lim, S.-J. Hwang, Y.S. Yoon, Y.H. Lee, J.-H. Choy, Adv. Funct. Mater. 17 (2007) 2949.
[16] S.H. Lee, T.W. Kim, D.H. Park, J.-H. Choy, S.-J. Hwang, N. Jiang, S.E. Park, Y.H. Lee, Chem. Mater. 19 (2007) 5010.
[17] D.H. Park, H.-W. Ha, S.H. Lee, J.-H. Choy, S.-J. Hwang, J. Phys. Chem. C 112 (2008) 5160.
[18] T.W. Kim, S.H. Lee, S.-J. Hwang, S.H. Hyun, J.-H. Choy, J. Nanosci. Nanotechnol. 7 (2007) 3857.
[19] A.-F. Wells, Structural Inorganic Chemistry, Clarendon Press, Oxford, 1984.
[20] J.-H. Choy, S.-J. Hwang, N.-G. Park, J. Am. Chem. Soc. 119 (1997) 1624.
[21] R.D. Shannon, Acta Crystallogr. A 32 (1976) 751.
[22] S.-J. Hwang, C.W. Kwon, J. Portier, G. Campet, H.S. Park, J.-H. Choy, P.V. Huong, M. Yoshimura, M. Kakihana, J. Phys. Chem. B 106 (2002) 4053.
[23] A. Manceau, A.I. Gorshkov, V.A. Drits, Am. Miner. 77 (1992) 1133.
[24] M. Schindler, F.C. Hawthorne, W.H. Bauer, Chem. Mater. 12 (2000) 1248.
[25] P. Chaurand, J. Rose, V. Briois, M. Salome, O. Proux, V. Nassif, L. Olivi, J. Susuni, J.-L. Hazemann, J.-Y. Bottero, J. Phys. Chem. B 111 (2007) 5101.
[26] N. Kumagai, H. Ooto, N. Kumagai, J. Power Sources 68 (1997) 600.
[27] M.Y. Song, D.S. Ahn, S.-G. Kang, S.H. Chang, Solid State Ionics 111 (1998) 237.
[28] M.M. Thackeray, M.F. Mansuetto, J.B. Bates, J. Power Sources 68 (1997) 153.